High-precision Monte Carlo study of several models in the three-dimensional U(1) universality class

Wanwan Xu,[1] Yanan Sun,[1] Jian-Ping Lv,[1,*] and Youjin Deng[2,3]

[1]*Anhui Key Laboratory of Optoelectric Materials Science and Technology, Key Laboratory of Functional Molecular Solids, Ministry of Education, Anhui Normal University, Wuhu, Anhui 241000, China*

[2]*Hefei National Laboratory for Physical Sciences at Microscale and Department of Modern Physics, University of Science and Technology of China, Hefei, Anhui 230026, China*

[3]*CAS Center for Excellence and Synergetic Innovation Center in Quantum Information and Quantum Physics, University of Science and Technology of China, Hefei, Anhui 230026, China*

(Received 16 June 2019; published 28 August 2019)

We present a worm-type Monte Carlo study of several typical models in the three-dimensional (3D) U(1) universality class, which include the classical 3D XY model in the directed flow representation and its Villain version, as well as the 2D quantum Bose-Hubbard (BH) model with unitary filling in the imaginary-time world-line representation. From the topology of the configurations on a torus, we sample the superfluid stiffness ρ_s and the dimensionless wrapping probability R. From the finite-size scaling analyses of ρ_s and of R, we determine the critical points as $T_c(\mathrm{XY}) = 2.201\,844\,1(5)$ and $T_c(\mathrm{Villain}) = 0.333\,067\,04(7)$ and $(t/U)_c(\mathrm{BH}) = 0.059\,729\,1(8)$, where T is the temperature for the classical models, and t and U are, respectively, the hopping and on-site interaction strength for the BH model. The precision of our estimates improves significantly over that of the existing results. Moreover, it is observed that at criticality, the derivative of a wrapping probability with respect to T suffers from negligible leading corrections and enables a precise determination of the correlation length critical exponent as $\nu = 0.671\,83(18)$. In addition, the critical exponent η is estimated as $\eta = 0.038\,53(48)$ by analyzing a susceptibilitylike quantity. We believe that these numerical results would provide a solid reference in the study of classical and quantum phase transitions in the 3D U(1) universality, including the recent development of the conformal bootstrap method.

DOI: 10.1103/PhysRevB.100.064525

I. INTRODUCTION

The U(1) criticality is a textbook example of phase transition and plays a crucial role in many-body phenomena ranging from vortex binding-unbinding transition [1], exotic quantum phases such as superfluid (SF) [2] and spin liquid [3,4], emergent continuous symmetries responsible for deconfined criticality [5,6] to quantum emulating [7] and to relativistic gauge field theories in particle physics [8]. Hence, the quantitative aspects of the U(1) criticality are frequently a requisite.

In three dimensions, systems within the U(1) universality class have a continuous phase transition with nontrivial critical exponents. Exact results are unavailable either for the critical points or the critical exponents. Numerical [9–14] and approximate [15–17] methodologies have been extensively applied. Up to now, the most precise estimates of critical exponents were obtained mostly with Monte Carlo methods, including $\nu = 0.671\,7(1)$ [11] and $0.671\,7(3)$ [12] and $\eta = 0.038\,1(2)$ [11]. These estimates have been extensively utilized in literature, albeit the estimate of ν differs from the celebrated experimental result $\nu = 0.670\,9(1)$ [18] determined by a specific heat measurement around the finite-temperature SF transition of ^{4}He performed in the microgravity environment of a space shuttle. The conformal bootstrap method has given a very precise determination for the critical exponents of the three-dimensional (3D) Ising ($\mathbb{Z}_2$) model, yet produced less precise estimates $\nu = 0.671\,9(11)$ and $\eta = 0.038\,52(64)$ for the U(1) case [17]. A summary of estimated critical exponents ν and η for the 3D U(1) universality class are given by Table I.

In this work we carry out a high-precision Monte Carlo study of three paradigmatic models in the 3D U(1) universality class, including the classical XY and Villain models on the simple-cubic lattice and the quantum Bose-Hubbard (BH) model with unitary filling on the square lattice. The XY model is the $n = 2$ case of the O(n) vector model and is a prototype of lattice models with continuous symmetries. It has a broad realm of physical realizations including granular superconductors and Josephson junction arrays [19]. The XY model has been extensively studied by Monte Carlo simulations, which are mostly on the spin representation and use the celebrated cluster update schemes [20,21]. The Villain model is a variant of the XY model. Both the XY and Villain models can be rewritten in the directed flow representation and then be simulated by the worm algorithm [22], which is very efficient in the measurement of correlation functions. Together with numerical analytical-continuation methods, the high-precision Monte Carlo data of the two-point correlation function, obtained by worm-type simulations, have uncovered intriguing low-energy excitations and transport properties near the critical temperature T_c [23,24]. It was observed [23] that the precise determination of T_c is crucial in these studies. The BH model and its extensions can describe a wide variety of quantum phenomena [25], including the SF, Mott insulator,

*jplv2014@ahnu.edu.cn

TABLE I. Estimates of the critical exponents ν and η in the 3D U(1) universality class. The method adopted and the year when the result was published are also listed. 'Ref.,' 'RG,' 'Exp.,' 'HTE,' 'MC,' and 'CB' are the abbreviations of 'reference,' 'renormalization group,' 'experiment,' 'high-temperature expansion,' 'Monte Carlo,' and 'conformal bootstrap,' respectively.

Ref.	Method	Year	ν	η
[15]	RG	1993	0.662(7)	
[30]	Exp.	1996	0.670 19(13)	
[16]	HTE	2000	0.671 66(55)	0.038 1(3)
[9]	MC	2001	0.671 6(5)	0.038 0(5)
[9]	MC+HTE	2001	0.671 55(27)	0.038 0(4)
[18]	Exp.	2003	0.670 9(1)	
[11]	MC+HTE	2006	0.671 7(1)	0.038 1(2)
[12]	MC	2006	0.671 7(3)	
[13]	MC (GPU)	2012	0.670 98(16)	
[13]	MC (GPU)	2012	0.671 38(11)	
[14]	MC (GPU)	2014	0.672(4)	
[17]	CB	2016	0.671 9(11)	0.038 52(64)
this work	MC	2019	0.671 83(18)	0.038 53(48)

TABLE II. Estimates of the critical temperatures for the 3D XY and Villain models and the critical hopping amplitude for the two-dimensional (2D) unitary-filling BH model. 'SCE' is the abbreviation of 'strong-coupling expansion.'

Model	Ref.	Method	Year	T_c or $(t/U)_c$
XY	[15]	MC	1993	2.201 67(10)
	[32]	MC	1996	2.201 843(19)
	[33]	MC	2002	2.201 833(19)
	[31]	MC	2005	2.201 840 5(48)
	[13]	MC (GPU)	2012	2.201 831 2(6)
	[13]	MC (GPU)	2012	2.201 852(1)
	[14]	MC (GPU)	2014	2.201 836(6)
	this work	MC	2019	2.201 844 1(5)
Villain	[34]	MC	2003	0.333 05(5)
	[23]	MC	2014	0.333 067 0(2)
	this work	MC	2019	0.333 067 04(7)
BH	[28]	SCE	1993	0.059 74(4)
	[29]	MC	2008	0.059 74(3)
	this work	MC	2019	0.059 729 1(8)

supersolid, and spin-liquid phases. In quantum Monte Carlo (QMC) simulations, the BH model is frequently expressed in terms of the imaginary-time world-line (path-integral) representation. In the field of cold-atom physics, the BH model has become a prominent object of state-of-the-art optical lattice emulators [7,26,27]. At unitary filling, i.e., each lattice site is occupied by a particle on average, the d-dimensional BH model exhibits the particle-hole symmetry, and the quantum phase transition between the SF and the Mott insulating phase belongs to the $(d+1)$-dimensional XY universality.

In our worm-type Monte Carlo simulations, periodic boundary conditions are applied. From the topology of the directed flow and the world-line configurations, we sample the SF stiffness ρ_s and the wrapping probabilities R's, of which the definitions will be given below. The data of ρ_s and R are analyzed according to the finite-size scaling theory and yield mutually consistent determinations of the critical points. The wrapping probability is observed to suffer from smaller finite-size corrections. The final estimates of the critical temperature, which takes into account both the statistical and the systematic uncertainties, are $T_c(\mathrm{XY}) = 2.201\,844\,1(5)$ and $T_c(\mathrm{Villain}) = 0.333\,067\,04(7)$. In a similar way, the quantum critical point (QCP) of the unitary-filling BH model is determined as $(t/U)_c = 0.059\,729\,1(8)$, where t is the hopping amplitude between the nearest-neighboring sites and U denotes the strength of on-site repulsion. Our estimates improve significantly over the existing results; see Table II for details. For instance, in comparison with $(t/U)_c = 0.059\,74(4)$ from the strong-coupling expansion [28] and $(t/U)_c = 0.059\,74(3)$ by QMC simulations [29], our result of the QCP has a higher precision by a factor of more than 40. To determine the correlation length critical exponent ν, we calculate the derivative of the wrapping probability R with respect to the temperature T from the covariance of R and energy. For the Villain model at criticality, a quantity of this type is found to exhibit negligible finite-size corrections and yields $\nu = 0.671\,83(18)$. This estimate is consistent with the most precise Monte Carlo results $\nu = 0.671\,7(1)$ [11] and $0.671\,7(3)$ [12] with a comparable precision and suggests that the experimental determination $\nu = 0.670\,9(1)$ [18] and the graphics processing unit (GPU) simulation result $\nu = 0.670\,98(16)$ [13] are unlikely. In addition, we obtain the critical exponent $\eta = 0.038\,53(48)$ from a susceptibilitylike quantity, which is very close to a recent conformal bootstrap estimate $\eta = 0.038\,52(64)$ [17].

In the remainder of this paper, we present details for the definition of the models, the methodology, and the scaling analyses of numerical results. Section II introduces the models addressed in this work. Section III elaborates the methodology which contains a unified formulation of worm Monte Carlo algorithm for the XY and Villain models, the definitions of sampled quantities, and finite-size scaling ansatze. Section IV presents Monte Carlo results and scaling analyzes. A short summary is finally given in Sec. V.

II. MODELS

The Hamiltonian of the XY model reads

$$H_{\mathrm{XY}} = -\sum_{\langle \mathbf{r}\mathbf{r}'\rangle} \mathbf{S}_{\mathbf{r}} \cdot \mathbf{S}_{\mathbf{r}'}, \tag{1}$$

where $\mathbf{S}_{\mathbf{r}} = (\cos\theta_{\mathbf{r}}, \sin\theta_{\mathbf{r}})$ denotes a planar spin vector with unit length at site $\mathbf{r}$ and the summation runs over pairs of nearest neighboring sites on a simple-cubic lattice. As listed in Table II, the most recent estimates of T_c (we have set $k_{\mathrm{B}} = 1$ for convenience) include 2.201 840 5(48) [31], 2.201 831 2(6) [13], 2.201 852(1) [13], and 2.201 836(6) [14]. Albeit these estimates are all based on Monte Carlo simulations, they are *not* completely consistent with each other.

We perform a high-temperature expansion on model (1) for the directed flow representation. We begin with the partition function

$$\mathcal{Z}_{\mathrm{XY}} = \left(\frac{1}{2\pi}\right)^N \int e^{-\frac{H_{\mathrm{XY}}}{T}} \prod_{\mathbf{r}} d\theta_{\mathbf{r}}, \tag{2}$$

where N is the number of lattice sites on the simple-cubic lattice and the exponential $e^{-\frac{H_{\rm XY}}{T}}$ can be expanded as

$$e^{-\frac{H_{\rm XY}}{T}} = \prod_{\langle \mathbf{r}\mathbf{r}'\rangle} e^{\frac{\cos(\theta_{\mathbf{r}}-\theta_{\mathbf{r}'})}{T}}. \tag{3}$$

Next, we combine (2) and (3) with the Fourier transform

$$e^{\frac{\cos(\theta_{\mathbf{r}}-\theta_{\mathbf{r}'})}{T}} = \sum_{\mathcal{C}_{\mathbf{r}\mathbf{r}'}=-\infty}^{+\infty} J_{\mathcal{C}_{\mathbf{r}\mathbf{r}'}}\left(\frac{1}{T}\right) e^{i\mathcal{C}_{\mathbf{r}\mathbf{r}'}(\theta_{\mathbf{r}}-\theta_{\mathbf{r}'})}, \tag{4}$$

where $J_{\mathcal{C}_{\mathbf{r}\mathbf{r}'}}(\frac{1}{T})$ represents the $\mathcal{C}_{\mathbf{r}\mathbf{r}'}$th order modified Bessel function of the first kind in variable of $\frac{1}{T}$; $J_{\mathcal{C}_{\mathbf{r}\mathbf{r}'}}(\frac{1}{T}) = J_{-\mathcal{C}_{\mathbf{r}\mathbf{r}'}}(\frac{1}{T})$. It follows that

$$\begin{aligned}
\mathcal{Z}_{\rm XY} &= \left(\frac{1}{2\pi}\right)^N \sum_{\{\mathcal{C}_{\mathbf{r}\mathbf{r}'}\}} \int \left(\prod_{\langle \mathbf{r}\mathbf{r}'\rangle} J_{\mathcal{C}_{\mathbf{r}\mathbf{r}'}}\left(\frac{1}{T}\right) e^{i\mathcal{C}_{\mathbf{r}\mathbf{r}'}(\theta_{\mathbf{r}}-\theta_{\mathbf{r}'})}\right) \prod_{\mathbf{r}} d\theta_{\mathbf{r}} \\
&= \left(\frac{1}{2\pi}\right)^N \sum_{\{\mathcal{C}_{\mathbf{r}\mathbf{r}'}\}} \left(\prod_{\langle \mathbf{r}\mathbf{r}'\rangle} J_{\mathcal{C}_{\mathbf{r}\mathbf{r}'}}\left(\frac{1}{T}\right)\right) \\
&\quad \times \int \prod_{\langle \mathbf{r}\mathbf{r}'\rangle} e^{i\mathcal{C}_{\mathbf{r}\mathbf{r}'}(\theta_{\mathbf{r}}-\theta_{\mathbf{r}'})} \prod_{\mathbf{r}} d\theta_{\mathbf{r}} \\
&= \left(\frac{1}{2\pi}\right)^N \sum_{\{\mathcal{C}_{\mathbf{r}\mathbf{r}'}\}} \left(\prod_{\langle \mathbf{r}\mathbf{r}'\rangle} J_{\mathcal{C}_{\mathbf{r}\mathbf{r}'}}\left(\frac{1}{T}\right)\right) \int \prod_{\mathbf{r}} e^{i\mathcal{D}_{\mathbf{r}}\theta_{\mathbf{r}}} \prod_{\mathbf{r}} d\theta_{\mathbf{r}}.
\end{aligned}$$

We represent the term $\mathcal{C}_{\mathbf{r}\mathbf{r}'}(\theta_{\mathbf{r}}-\theta_{\mathbf{r}'})$ by a vector flow variable $\mathcal{C}_{\mathbf{r}\mathbf{r}'}$ from $\mathbf{r}$ to $\mathbf{r}'$. As $\mathcal{C}_{\mathbf{r}\mathbf{r}'}$ is positive (negative), it means that the flow is from $\mathbf{r}$ to $\mathbf{r}'$ ($\mathbf{r}'$ to $\mathbf{r}$); $\mathcal{C}_{\mathbf{r}\mathbf{r}'} = -\mathcal{C}_{\mathbf{r}'\mathbf{r}}$. $\mathcal{D}_{\mathbf{r}} = \sum_{\mathbf{r}'} \mathcal{C}_{\mathbf{r}\mathbf{r}'}$ denotes the divergence of flow at $\mathbf{r}$. The inner integration would be zero unless $\Delta\mathcal{C} = 0 := (\forall\ \mathbf{r}, \mathcal{D}_{\mathbf{r}} = 0)$. Hence $\Delta\mathcal{C} = 0$ represents the null divergence of flow over lattice sites and mimics the Kirchhoff's current law. As a result we have

$$\mathcal{Z}_{\rm XY} = \sum_{\Delta\mathcal{C}=0} \prod_{\langle \mathbf{r}\mathbf{r}'\rangle} J_{\mathcal{C}_{\mathbf{r}\mathbf{r}'}}\left(\frac{1}{T}\right), \tag{5}$$

where the summation runs over all the directed flow states with $\Delta\mathcal{C} = 0$. Up to now, we have finished an exact transformation of standard XY model onto a directed flow model, for which we illustrate a configuration in Fig. 1.

A variant of the standard XY model is the Villain model with partition function

$$\mathcal{Z}_{\rm Villain} = \left(\frac{1}{2\pi}\right)^N \int \prod_{\mathbf{r}} d\theta_{\mathbf{r}} \sum_{\mathcal{L}_{\mathbf{r}\mathbf{r}'}=-\infty}^{+\infty} e^{-\frac{1}{2T}\sum_{\langle \mathbf{r}\mathbf{r}'\rangle}(\theta_{\mathbf{r}'}-\theta_{\mathbf{r}}-2\pi\mathcal{L}_{\mathbf{r}\mathbf{r}'})^2}. \tag{6}$$

The 2π periodicity persists in the interaction potential of the Villain model, which is believed to capture the characteristics of the XY model [23,24,34–36]. A high-temperature expansion [37] can be performed on the Villain model to build the directed flow representation. As a result, the partition function

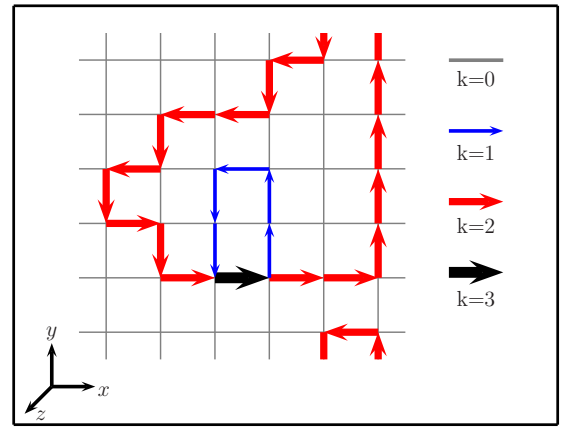

FIG. 1. A directed flow configuration of the XY and Villain models on a cross section of $6 \times 6 \times 6$ periodic simple-cubic lattice.

in the directed flow space $\Delta\mathcal{C} = 0$ reads

$$\mathcal{Z}_{\rm Villain} = \sum_{\Delta\mathcal{C}=0} \prod_{\langle \mathbf{r}\mathbf{r}'\rangle} e^{\frac{-\mathcal{C}^2_{\mathbf{r}\mathbf{r}'}}{2T}}. \tag{7}$$

Note that the Villain model has a simple form of statistical weight allocation in the directed flow representation. Estimates of T_c for the 3D Villain model are summarized in Table II.

We consider the 2D unitary-filling BH model with the Hamiltonian

$$\hat{H}_{\rm BH} = -t \sum_{\langle \mathbf{r}\mathbf{r}'\rangle} (\hat{a}^+_{\mathbf{r}}\hat{a}_{\mathbf{r}'} + \hat{a}^+_{\mathbf{r}'}\hat{a}_{\mathbf{r}}) + \frac{U}{2} \sum_{\mathbf{r}} \hat{n}_{\mathbf{r}}(\hat{n}_{\mathbf{r}} - 1), \tag{8}$$

where $\hat{a}^+_{\mathbf{r}}$ ($\hat{a}_{\mathbf{r}}$) represents the local bosonic creation (annihilation) operator at site $\mathbf{r}$; $\hat{n}_{\mathbf{r}}{=}\hat{a}^+_{\mathbf{r}}\hat{a}_{\mathbf{r}}$. The first summation runs over the pairs of nearest-neighboring sites on a square lattice and the second one is over sites. When the particle density is fixed at integer numbers, a quantum phase transition between the compressible SF phase and the incompressible Mott insulating phase occurs by tuning the ratio t/U. The transition falls in the 3D U(1) universality and features a relativistic (particle-hole) symmetry with the dynamical critical exponent $z = 1$. In this work we study the unitary-filling case for which the QCP has been estimated as $(t/U)_c = 0.059\,74(4)$ by a high-order strong-coupling expansion [28] and $(t/U)_c = 0.059\,74(3)$ by QMC simulations [29]. These two estimates have become benchmarks for the location of QCP of the 2D unitary-filling BH model (Table II).

III. METHODOLOGY

A. Monte Carlo algorithms

Our Monte Carlo simulations of both the classical (XY and Villain) and quantum (BH) models employ worm-type algorithms. For the classical models the worm algorithm was first proposed in Ref. [22]. An explicit formulation of worm algorithm for the Villain model has been presented in Ref. [34]. It has been demonstrated [38] that the worm algorithm stands out from state-of-the-art algorithms when sampling certain quantities for the 3D Ising model. For completeness, we shall formulate a worm algorithm for the XY

and Villain models. As for the BH model, we use the standard worm QMC algorithm in the continuous imaginary time path-integral (world-line) representation [39,40], for which we refrain from a detailed elaboration and refer the readers to Refs. [39–42].

1. Worm algorithm for the XY model

Extending state space. A character of worm algorithm is enlarging state space. It extends the original directed flow space $\Delta\mathcal{C}=0$ by including two additional degrees of freedom, namely, two defects I and M individually on a site, by defining that the subspace with $I=M$ recovers exactly the original space $\Delta\mathcal{C}=0$ and that the subspace with $I\neq M$ is exactly outside the original space. The latter is called worm ($\mathcal{W}$) sector, where the Kirchhoff's current law does not hold for sites I and M, namely, $\mathcal{D}_I\neq 0$, $\mathcal{D}_M\neq 0$. Accordingly, the partition function for the extended state space can be separated into two parts [43]. The first part

$$\mathcal{Z}_{\mathrm{XY}}=\frac{1}{N}\sum_{\Delta\mathcal{C}=0;I,M}\delta_{I,M}\prod_{\langle\mathbf{r}\mathbf{r}'\rangle}J_{\mathcal{C}_{\mathbf{r}\mathbf{r}'}}\left(\frac{1}{T}\right) \tag{9}$$

corresponds to the original partition function (5), with δ the Kronecker delta function. The summation runs over the extended state space. The second part relates to $\mathcal{W}$ sector and reads

$$\mathcal{Z}_{\mathcal{W}}=\frac{1}{N}\sum_{\Delta\mathcal{C}=0;I,M}(1-\delta_{I,M})\prod_{\langle\mathbf{r}\mathbf{r}'\rangle}J_{\mathcal{C}_{\mathbf{r}\mathbf{r}'}}\left(\frac{1}{T}\right). \tag{10}$$

The Monte Carlo simulations will be performed in the extended state space with the partition function

$$\mathcal{Z}_{\mathrm{Ext}}=\mathcal{Z}_{\mathrm{XY}}+\Lambda\mathcal{Z}_{\mathcal{W}}, \tag{11}$$

where Λ is a tunable parameter often (but not necessarily) set as $\Lambda=1$.

Worm updates. The worm process moves I or/and M around the lattice and updates the directed flow configuration by changing the local flow variable through a biased random walk designed with detailed balance. More specifically, as I (M) moves to a neighboring site $I_{\mathcal{N}}$ ($M_{\mathcal{N}}$), the flow on edge $II_{\mathcal{N}}$ ($MM_{\mathcal{N}}$) will be updated accordingly by adding a unit, directed flow from I to $I_{\mathcal{N}}$ ($M_{\mathcal{N}}$ to M). The movement repeats until I and M meet ($I=M$), when the original state space is hit. Hence the movement of I or M serves as a step of random walk in the $\mathcal{W}$ sector or in between the $\mathcal{W}$ sector and the original state space. The core steps are given as follows.

Core steps of the worm algorithm for the XY model

Step 1. If $I=M$, randomly choose a new site I' and set $I=M=I'$, $\mathrm{sign}(I)=1$, $\mathrm{sign}(M)=-1$.

Step 2. Interchange $I\leftrightarrow M$ and $\mathrm{sign}(I)\leftrightarrow\mathrm{sign}(M)$ with probability $1/2$.

Step 3. Randomly choose one neighboring site $I_{\mathcal{N}}$ of I.

Step 4. Propose to move $I\rightarrow I_{\mathcal{N}}$ by updating the flow along edge-$II_{\mathcal{N}}$, $\mathcal{C}_{II_{\mathcal{N}}}$, to $\mathcal{C}'_{II_{\mathcal{N}}}$:

$$\mathcal{C}'_{II_{\mathcal{N}}}=\mathcal{C}_{II_{\mathcal{N}}}+\mathrm{sign}(I\rightarrow I_{\mathcal{N}})\mathrm{sign}(I),$$

where $\mathrm{sign}(I\rightarrow I_{\mathcal{N}})=\pm 1$, parametrizing the flow direction along edge-$II_{\mathcal{N}}$.

Step 5. Accept the proposal with probability

$$\mathbf{P}_{\mathrm{acc}}=\min\left(1,\frac{J_{\mathcal{C}'_{II_{\mathcal{N}}}}\left(\frac{1}{T}\right)}{J_{\mathcal{C}_{II_{\mathcal{N}}}}\left(\frac{1}{T}\right)}\right)$$

according to the Metropolis scheme.

Monte Carlo simulations are constituted by repeating steps 1 to 5. The exploration of the XY model is achieved by sampling quantities as the original state space is hit. Besides, the worm process itself is informative for detecting two-point correlations. A susceptibilitylike quantity T_w (integral of two-point correlation) can be evaluated by the number of worm steps between subsequent hits on the original state space, which is known as returning time τ_{w}. Accordingly, the definition of T_w is given by

$$T_w=\langle\tau_w\rangle, \tag{12}$$

which scales as $T_w\sim L^{2-\eta}$ at the critical point and is useful for determining the critical exponent η.

2. Worm algorithm for the Villain model

The worm algorithm formulated in Sec. III A 1 applies to the Villain model once a substitute of *step* 5 is taken as follows.

Step 5. Accept the proposal with probability

$$\mathbf{P}_{\mathrm{acc}}=\min\left(1,e^{\frac{-(\mathcal{C}'^2_{II_{\mathcal{N}}}-\mathcal{C}^2_{II_{\mathcal{N}}})}{2T}}\right)$$

according to the Metropolis scheme.

The definition of T_w (12) applies to the Villain model as well.

B. Sampled quantities

Wrapping probability has been studied for random cluster models (including its limiting situations percolation, Ising and Potts models, etc.) [44–52]. Thus far, however, the method has not been employed for the U(1) lattice models which, as we have shown, admit a graphic representation such as directed flow representation. Moreover, the applicability of wrapping probability approach to quantum models has not yet been addressed.

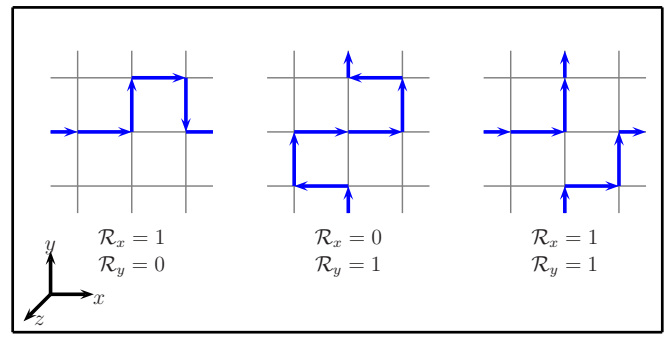

FIG. 2. Illustration of wrappings for directed flow configurations of the 3D XY and Villain models on a cross section of $3\times 3\times 3$ periodic simple-cubic lattice.

TABLE III. Fits of the wrapping probabilities R_x, R_a, R_2 to (24) and the scaled SF stiffness $\rho_s L$ to (28) for the 3D Villain model. 'Qua.' is the abbreviation of 'quantities.' The correction exponents $\omega_1 = 0.789$ and $\omega_2 = 1.77$ are adopted. The symbol '—' denotes the absence of the corresponding correction term in the fit.

Qua.	$L_{\min}$	χ^2/DF	T_c	$1/\nu$	$\mathcal{Q}_0$	a_1	b_1	b_2
	16	27.2/26	0.333 067 035(15)	1.43(6)	0.378 65(4)	−1.26(39)	−0.0459(4)	–
	24	24.8/22	0.333 067 038(16)	1.43(6)	0.378 66(5)	−1.32(41)	−0.0461(7)	–
	32	22.0/18	0.333 067 039(17)	1.43(6)	0.378 67(6)	−1.31(41)	−0.046(1)	–
R_x	64	21.0/14	0.333 067 045(22)	1.43(6)	0.378 7(1)	−1.31(43)	−0.047(3)	–
	8	29.1/29	0.333 067 047(16)	1.44(6)	0.378 72(5)	−1.25(38)	−0.0480(9)	0.025(5)
	16	26.9/25	0.333 067 041(18)	1.44(6)	0.378 68(7)	−1.25(39)	−0.047(2)	0.01(2)
	24	24.7/21	0.333 067 041(21)	1.43(6)	0.378 7(1)	−1.31(41)	−0.047(4)	0.02(7)
	32	21.9/17	0.333 067 044(25)	1.43(6)	0.378 7(2)	−1.30(41)	−0.048(7)	0.04(14)
	24	33.5/22	0.333 067 020(18)	1.41(6)	0.688 70(7)	−1.90(65)	−0.031(1)	–
	32	23.3/18	0.333 067 032(19)	1.42(6)	0.688 79(8)	−1.78(62)	−0.033(2)	–
R_a	64	20.7/14	0.333 067 044(24)	1.42(7)	0.688 9(2)	−1.81(65)	−0.037(4)	–
	8	34.9/29	0.333 067 058(18)	1.43(6)	0.689 05(7)	−1.73(59)	−0.044(1)	0.194(8)
	16	33.0/25	0.333 067 046(20)	1.43(6)	0.689 0(1)	−1.72(59)	−0.040(3)	0.15(3)
	24	29.9/21	0.333 067 050(24)	1.42(6)	0.689 0(2)	−1.83(63)	−0.042(6)	0.19(10)
	32	22.8/17	0.333 067 046(28)	1.43(6)	0.689 0(3)	−1.76(62)	−0.04(1)	0.14(21)
	16	31.7/26	0.333 067 074(21)	1.47(9)	0.264 10(4)	−0.81(37)	−0.034 7(5)	–
	24	16.1/22	0.333 067 060(23)	1.47(9)	0.264 06(5)	−0.83(39)	−0.033 8(8)	–
	32	13.5/18	0.333 067 059(25)	1.47(9)	0.264 05(6)	−0.82(39)	−0.034(1)	–
R_2	64	12.2/14	0.333 067 049(31)	1.46(9)	0.264 0(1)	−0.89(43)	−0.032(3)	–
	8	31.2/29	0.333 067 062(23)	1.47(9)	0.264 06(5)	−0.83(38)	−0.033 3(9)	−0.015(6)
	16	29.1/25	0.333 067 050(26)	1.47(9)	0.264 00(8)	−0.82(38)	−0.032(2)	−0.04(2)
	24	16.0/21	0.333 067 052(31)	1.47(9)	0.264 0(1)	−0.84(39)	−0.032(4)	−0.03(7)
	32	13.0/17	0.333 067 041(36)	1.47(9)	0.263 9(2)	−0.82(39)	−0.029(8)	−0.10(15)
	16	30.4/26	0.333 067 019(15)	1.45(6)	0.515 45(6)	−2.21(67)	−0.1452(8)	–
	24	25.5/22	0.333 067 028(16)	1.44(6)	0.515 51(8)	−2.30(70)	−0.146(1)	–
	32	24.7/18	0.333 067 029(18)	1.43(6)	0.515 5(1)	−2.38(74)	−0.147(2)	–
$\rho_s L$	64	24.0/14	0.333 067 035(22)	1.43(6)	0.515 6(2)	−2.39(76)	−0.149(5)	–
	8	30.0/29	0.333 067 040(16)	1.45(6)	0.515 66(8)	−2.14(65)	−0.152(2)	0.078(9)
	16	28.5/25	0.333 067 034(18)	1.45(6)	0.515 6(1)	−2.17(66)	−0.150(3)	0.05(4)
	24	25.4/21	0.333 067 033(22)	1.44(6)	0.515 6(2)	−2.28(70)	−0.149(7)	0.04(12)
	32	24.7/17	0.333 067 033(26)	1.43(6)	0.515 6(3)	−2.38(74)	−0.15(1)	0.05(24)

The original definition of wrapping is based on the cluster representation of percolation [44]. Here we extend its original definition to describe a broader class of graphic representation constituted by the directed flows (XY and Villain models) or the particle lines in the imaginary-time path-integral configuration (BH model) by exploiting the wrapping of directed flows or particle lines around the lattice torus. As the flow is nondivergent, the wrapping for XY and Villain models around a certain direction can be justified by the presence of *net* flow passing through the perpendicular cross section. Moreover, in the present worm Monte Carlo simulations for the XY, Villain, and BH models, the wrapping of directed flows or particle lines can be justified by tracking the movements of defects (I and M). Directed flow configurations with wrapping, namely, $\mathcal{R}_\kappa = 1$ for $\kappa = x, y,$ or/and z, are illustrated by Fig. 2 for XY and Villain models.

TABLE IV. Fits of T_w to (32) for the 3D Villain model. The correction exponents $\omega_1 = 0.789$ and $\omega_2 = 1.77$ are adopted.

$L_{\min}$	χ^2/DF	T_c	η	$1/\nu$	$\mathcal{Q}_0$	a_1	b_1	b_2
16	29.8/28	0.333 066 996(17)	0.0392(2)	1.52(4)	1.360(1)	−3.06(67)	−0.307(6)	–
24	24.2/24	0.333 067 021(21)	0.0386(4)	1.52(4)	1.356(2)	−3.04(67)	−0.29(1)	–
32	21.7/20	0.333 067 027(25)	0.0385(5)	1.53(4)	1.355(4)	−2.95(66)	−0.28(2)	–
64	21.1/15	0.333 067 027(55)	0.0385(16)	1.53(4)	1.36(1)	−2.90(66)	−0.28(9)	–
8	29.4/31	0.333 067 040(20)	0.0380(3)	1.52(4)	1.351(2)	−3.01(66)	−0.24(1)	−0.40(5)
16	26.1/27	0.333 067 042(29)	0.0379(7)	1.53(4)	1.351(5)	−2.96(65)	−0.24(4)	−0.4(2)
24	24.0/23	0.333 067 034(39)	0.0382(11)	1.52(4)	1.353(9)	−3.03(67)	−0.26(8)	−0.2(6)
32	21.7/19	0.333 067 027(67)	0.0385(25)	1.53(4)	1.36(2)	−2.95(66)	−0.3(2)	0(2)

1. Sampled quantities for the 3D XY and Villain models

Some wrapping-related quantities for 3D XY and Villain models are defined as follows. The wrapping probabilities in the directed flow representation are given by

$$R_x = \langle \mathcal{R}_x \rangle = \langle \mathcal{R}_y \rangle = \langle \mathcal{R}_z \rangle, \tag{13}$$

$$R_a = 1 - \langle (1-\mathcal{R}_x)(1-\mathcal{R}_y)(1-\mathcal{R}_z) \rangle, \tag{14}$$

$$R_2 = \langle \mathcal{R}_x \mathcal{R}_y (1-\mathcal{R}_z) \rangle + \langle \mathcal{R}_y \mathcal{R}_z (1-\mathcal{R}_x) \rangle + \langle \mathcal{R}_z \mathcal{R}_x (1-\mathcal{R}_y) \rangle, \tag{15}$$

where R_x, R_a, and R_2 define the probabilities that the wrapping of directed flows exists in x direction, in at least one direction and in two (and only two) directions, respectively. For a wrapping observable (say $\mathcal{R}_\kappa$), we define its covariance with energy $\mathcal{E}$ as

$$G_{R_\kappa E} = \frac{1}{T^2} (\langle \mathcal{R}_\kappa \mathcal{E} \rangle - \langle \mathcal{R}_\kappa \rangle \langle \mathcal{E} \rangle), \tag{16}$$

which is equivalent to the derivative of R_κ with respect to T.

Recall the definition of a winding number on a torus. If a direction (say κ) is specified, the event *wrapping* (namely, $\mathcal{R}_\kappa = 1$) relates to a nonzero winding number $\mathcal{W}_\kappa \neq 0$ of directed flow. The latter has a close connection to the definition of SF stiffness [53]. We sample the SF stiffness by winding number fluctuations, which can be written as

$$\rho_s = \langle \mathcal{W}_x^2 + \mathcal{W}_y^2 + \mathcal{W}_z^2 \rangle / 3L. \tag{17}$$

Moreover, we estimate the derivative of ρ_s with respect to T by

$$G_{\rho_s E} = \frac{1}{3LT^2} \big(\langle (\mathcal{W}_x^2 + \mathcal{W}_y^2 + \mathcal{W}_z^2) \mathcal{E} \rangle - \langle \mathcal{W}_x^2 + \mathcal{W}_y^2 + \mathcal{W}_z^2 \rangle \langle \mathcal{E} \rangle \big). \tag{18}$$

2. Sampled quantities for the 2D BH model

For the 2D BH model, the wrapping probabilities of particle lines in the world-line representation read

$$R_x = \langle \mathcal{R}_x \rangle = \langle \mathcal{R}_y \rangle, \tag{19}$$

$$R_a = 1 - \langle (1-\mathcal{R}_x)(1-\mathcal{R}_y) \rangle, \tag{20}$$

$$R_2 = \langle \mathcal{R}_x \mathcal{R}_y \rangle, \tag{21}$$

where R_x, R_a, and R_2 define the probabilities that the wrapping of particle lines exists in the x direction, in at least one direction, and in two directions, respectively. For a given spatial direction (say κ), the event *wrapping* (namely, $\mathcal{R}_\kappa = 1$) relates to a nonzero winding number $\mathcal{W}_\kappa \neq 0$ of particle lines. We sample the SF stiffness by winding number fluctuations through [53]

$$\rho_s = \langle \mathcal{W}_x^2 + \mathcal{W}_y^2 \rangle / 4t\beta. \tag{22}$$

C. Finite-size scaling ansatze

In order to formulate the finite-size scaling for the thermodynamic phase transition of the classical (XY and Villain) models and the quantum phase transition of the quantum (BH) model in a more or less unified manner, a quantum to classical mapping is required. For the QCP of the unitary-filling BH model, the dynamic critical exponent $z = 1$ [54] has been verified extensively [34,35]. In our QMC simulations of the BH model, we use the temperature contour $\beta \equiv 1/T = 2L$. This treatment eliminates the variable β/L^z in the finite-size scaling ansatz of the BH model.

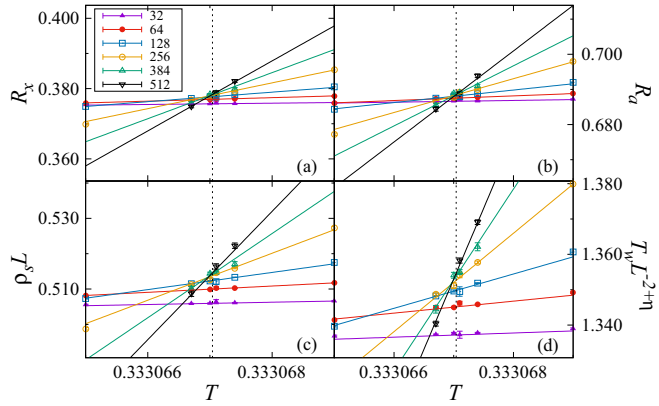

FIG. 3. Wrapping probabilities R_x and R_a, scaled SF stiffness $\rho_s L$ and scaled susceptibilitylike quantity $T_w L^{-2+\eta}$ versus T in the neighborhood of critical temperature for the 3D Villain model. The linear lattice sizes are $L = 32$, 64, 128, 256, 384, and 512. The symbols stand for Monte Carlo raw data, and the lines are drawn with a preferred fit with $\chi^2/\mathrm{DF} \approx 1$. Note that the same domain of vertical coordinate is focused on around the crossing points (estimated by $\mathcal{Q}_0$ in the fits) for the quantities to make it is fair to compare finite-size corrections. The vertical dashed lines represent our finite estimate of critical temperature $T_c = 0.333\,067\,04(7)$.

Wrapping probabilities are dimensionless quantities whose finite-size scaling is described by

$$R_\kappa = \widetilde{R}_\kappa (\epsilon L^{1/\nu}) \tag{23}$$

where $\widetilde{R}_\kappa$ is a scaling function, and ϵ denotes the distance to critical point. We set for the XY and Villain models $\epsilon = T_c - T$ and for the BH model $\epsilon = (t/U)_c - t/U$.

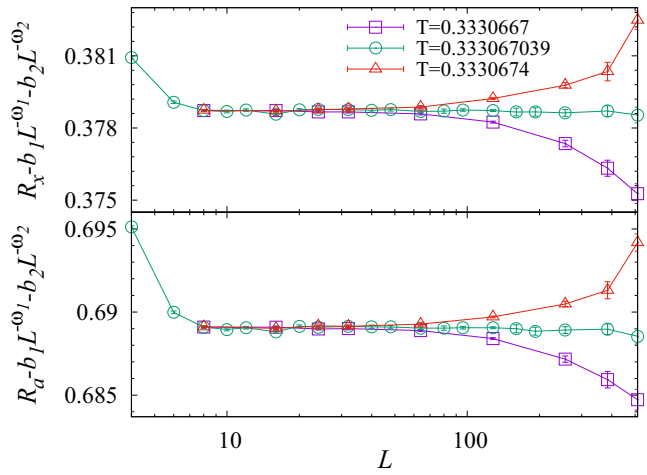

FIG. 4. Scaled R_x and R_a with correction terms versus L at T_c and its neighborhoods for the 3D Villain model. The corrections terms quote preferred fitting results in Table III.

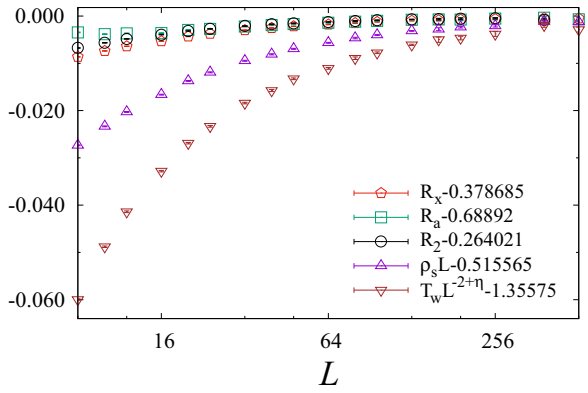

FIG. 5. Corrections to leading scaling revealed by $R_\kappa - \mathcal{Q}_0$ for R_κ ($\kappa = x, a, 2$), by $\rho_s L - \mathcal{Q}_0$ for $\rho_s L$, and by $T_w L^{-2+\eta} - \mathcal{Q}_0$ for T_w at the estimated critical temperature $T_c = 0.333\,067\,039$ of the 3D Villain model. The parameter $\mathcal{Q}_0$ is determined from Table III for R_κ ($\kappa = x, a, 2$) and $\rho_s L$, and from Table IV for T_w. The critical exponent η takes our finite estimate $\eta = 0.038\,53$.

Performing a Taylor's expansion and incorporating corrections to scaling, we have

$$R_\kappa = \mathcal{Q}_0 + \sum_n a_n \epsilon L^{n/\nu} + \sum_m b_m L^{-\omega_m}, \tag{24}$$

where $\mathcal{Q}_0$ is a somewhat universal constant, a_n ($n = 1, 2, ...$) and b_m ($m = 1, 2, ...$) are nonuniversal constants, and ω_m ($m = 1, 2, ...$) refers to correction-to-scaling exponents. To estimate the critical exponent ν we analyze $G_{R_\kappa E} = \frac{dR_\kappa}{dT}$ which should scale as

$$G_{R_\kappa E} = L^{1/\nu} \widetilde{G}_{R_\kappa E}(\epsilon L^{1/\nu}), \tag{25}$$

and we have

$$G_{R_\kappa E} = L^{1/\nu}\left(\mathcal{Q}_0 + \sum_n a_n \epsilon L^{n/\nu} + \sum_m b_m L^{-\omega_m}\right). \tag{26}$$

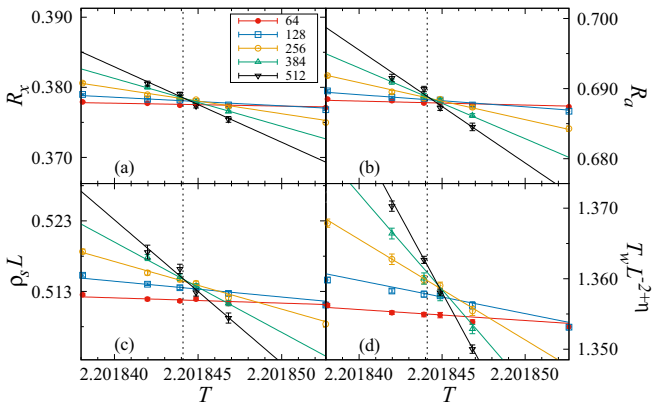

FIG. 6. Wrapping probabilities R_x and R_a, scaled SF stiffness $\rho_s L$, and scaled susceptibilitylike quantity $T_w L^{-2+\eta}$ versus T in the neighborhood of critical temperature for the 3D XY model. The linear lattice sizes are $L = 64$, 128, 256, 384, and 512. The same domain of vertical coordinate is focused on for the quantities. The vertical dashed lines represent our finite estimate of critical temperature $T_c = 2.201\,844\,1(5)$.

TABLE V. Critical wrapping probabilities R_x^c, R_a^c, R_2^c and critical winding number fluctuations $\rho_s^c L$ for the 3D Villain and XY models.

	Villain	XY
R_x^c	0.378 7(2)	0.378 8(4)
R_a^c	0.688 9(4)	0.688 9(6)
R_2^c	0.264 0(3)	0.264 1(5)
$\rho_s^c L$	0.515 6(3)	0.515 8(9)

The finite-size scaling of ρ_s can be figured out by $\rho_s \sim \xi^{2-d-z}$ [54,55] with ξ the correlation length. For the present case (three space-time dimensions), we have $d + z = 3$. It follows that

$$\rho_s L = \widetilde{\rho}_s(\epsilon L^{1/\nu}) \tag{27}$$

and

$$\rho_s L = \mathcal{Q}_0 + \sum_n a_n \epsilon L^{n/\nu} + \sum_m b_m L^{-\omega_m}. \tag{28}$$

The scaling form of $G_{\rho_s E} = \frac{d\rho_s}{dT}$ reads

$$G_{\rho_s E} = L^{(-1+\frac{1}{\nu})} \widetilde{G}_{\rho_s E}(\epsilon L^{1/\nu}), \tag{29}$$

and we have

$$G_{\rho_s E} = L^{(-1+\frac{1}{\nu})}\left(\mathcal{Q}_0 + \sum_n a_n \epsilon L^{n/\nu} + \sum_m b_m L^{-\omega_m}\right). \tag{30}$$

Besides, for the XY and Villain models, one may use the following scaling form of T_w to determine the critical exponent η,

$$T_w = L^{2-\eta} \widetilde{T}_w(\epsilon L^{1/\nu}), \tag{31}$$

which gives

$$T_w = L^{2-\eta}\left(\mathcal{Q}_0 + \sum_n a_n \epsilon L^{n/\nu} + \sum_m b_m L^{-\omega_m}\right). \tag{32}$$

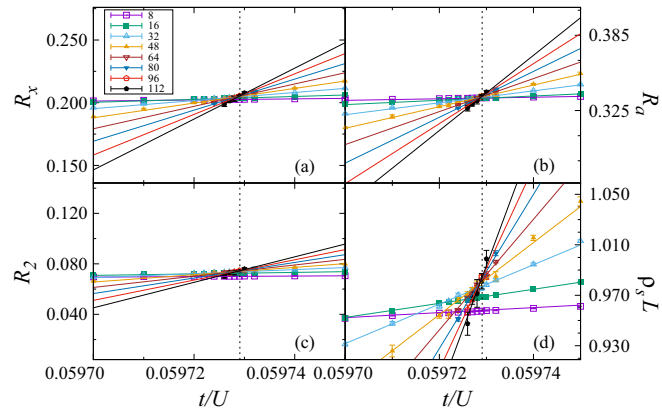

FIG. 7. Wrapping probabilities R_x, R_a, R_2 and scaled SF stiffness $\rho_s L$ in the neighborhood of QCP for the 2D unitary-filling BH model. The linear lattice sizes are $L = 8$, 16, 32, 48, 64, 80, 96, and 112; for each L, the inverse temperature is $\beta = 2L$. The same domain of vertical coordinate is focused on for the quantities. The vertical dashed lines represent our finite estimate of QCP, namely, $(t/U)_c = 0.059\,729\,1(8)$.

TABLE VI. Fits of G_{R_xE}, G_{R_aE}, G_{R_2E}, and G_{ρ_sE} to (33) at the estimated critical temperature $T_c = 0.333\,067\,039$ of the 3D Villain model. The correction exponent $\omega_1 = 0.789$ is adopted.

Qua.	$L_{\min}$	χ^2/DF	$1/\nu$	$\mathcal{Q}_0$	b_1
G_{R_xE}	16	17.4/13	1.488 47(14)	0.989 0(5)	–
	20	16.8/12	1.488 53(17)	0.988 8(7)	–
	24	14.5/11	1.488 38(20)	0.989 4(8)	–
	32	14.4/10	1.488 33(24)	0.990(1)	–
	40	11.3/9	1.488 66(31)	0.988(1)	–
	48	9.2/8	1.488 45(34)	0.989(2)	–
	16	17.4/12	1.488 49(54)	0.989(3)	0.001(13)
	20	16.4/11	1.488 13(64)	0.991(3)	−0.01(2)
	24	14.3/10	1.488 67(75)	0.988(4)	0.01(2)
	32	13.5/9	1.489 2(10)	0.985(5)	0.03(3)
	40	11.0/8	1.488 0(12)	0.992(7)	−0.03(5)
	48	9.1/7	1.488 9(14)	0.987(8)	0.02(6)
G_{R_aE}	16	15.0/12	1.487 82(62)	1.344(4)	0.10(2)
	20	13.5/11	1.487 32(74)	1.348(5)	0.08(3)
	24	10.9/10	1.488 01(85)	1.343(6)	0.11(4)
	32	10.3/9	1.488 5(11)	1.339(8)	0.14(5)
	40	8.7/8	1.487 5(14)	1.35(1)	0.07(8)
	48	8.4/7	1.487 9(15)	1.34(1)	0.1(1)
G_{R_2E}	16	16.7/12	1.489 18(72)	0.768(3)	0.10(1)
	20	16.5/11	1.488 96(86)	0.769(4)	0.09(2)
	24	14.9/10	1.489 6(10)	0.766(4)	0.11(2)
	32	11.8/9	1.491 1(13)	0.760(6)	0.16(4)
	40	10.0/8	1.489 6(17)	0.766(8)	0.10(6)
	48	9.9/7	1.489 9(19)	0.765(9)	0.11(7)
G_{ρ_sE}	16	16.7/12	1.488 42(54)	1.825(5)	−0.52(2)
	20	16.7/11	1.488 33(65)	1.826(6)	−0.53(3)
	24	15.2/10	1.488 83(77)	1.821(8)	−0.49(5)
	32	14.9/9	1.489 2(10)	1.82(1)	−0.47(7)
	40	13.0/8	1.488 1(12)	1.83(1)	−0.6(1)
	48	10.6/7	1.489 0(14)	1.82(1)	−0.5(1)

In principle, an analytic background should be added up to (31) and (32). For the present case, this analytic background is effectively higher-order corrections compared with the correction terms taken into account explicitly throughout this work.

IV. NUMERICAL RESULTS AND FINITE-SIZE SCALING ANALYSES

In this section, we present Monte Carlo results which are analyzed by performing finite-size scaling. In Sec. IV A, firstly, the scaling behaviors of wrapping probabilities and some other quantities are explored for 3D Villain and XY models. We find that certain wrapping probabilities exhibit smaller corrections in finite-size scaling than those of the "conventional" quantities such as SF stiffness and susceptibilitylike quantities. Universal values of critical dimensionless quantities are confirmed numerically for the XY and Villain models. Subsequently, we extend the wrapping probability approach to determine the QCP of the 2D unitary-filling BH model. For each of the Villain, XY, and BH models, an unprecedentedly precise estimate of critical point is obtained. In Sec. IV B, we determine the critical exponents ν and η following extensive simulations at the high-precision T_c of the Villain model. We find that the quantity G_{R_xE} exhibits a negligible (if nonzero) amplitude of leading correction, which helps to determine a precise estimate of critical exponent ν. Moreover, the critical exponent η is estimated by analyzing the susceptibilitylike quantity T_w.

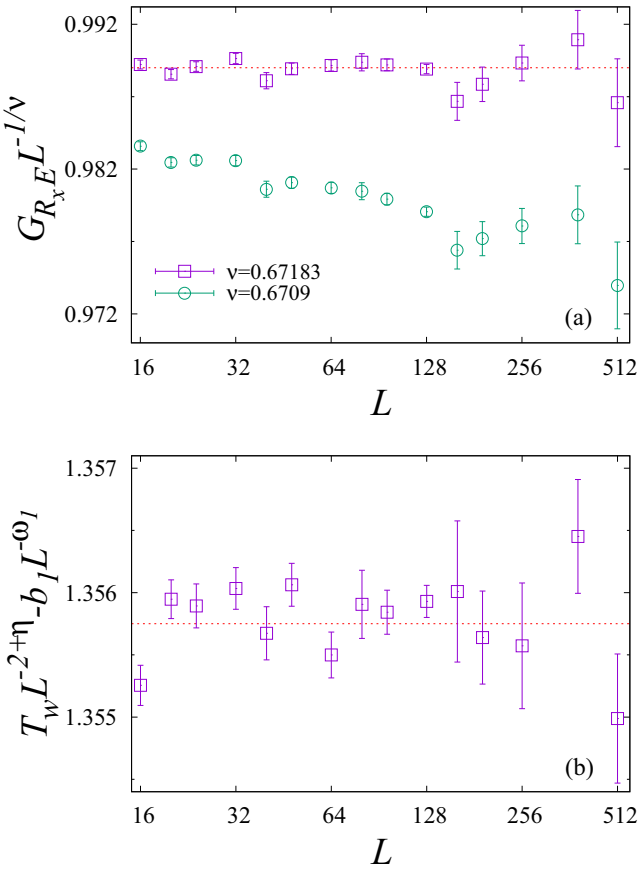

FIG. 8. (a) Scaled quantity $G_{R_xE}L^{-1/\nu}$ with $\nu = 0.671\,83$ (estimate of this work) and $\nu = 0.670\,9$ (experimental result [18]) at the estimated critical temperature $T_c = 0.333\,067\,039$ of the 3D Villain model. The horizonal dashed line denotes $\mathcal{Q}_0 = 0.989$ which is determined from Table VI. (b) Scaled quantity $T_wL^{-2+\eta}$ with $\eta = 0.038\,53$. A correction term quoted from Table VII is included. The horizonal dashed line denotes $\mathcal{Q}_0 = 1.355\,75$ which is determined from Table IV.

A. Determining critical points

1. 3D Villain model

We simulate the 3D Villain model on periodic $L \times L \times L$ simple-cubic lattices with linear sizes $L = 16$, 24, 32, 64, 128, 256, 384, and 512 for different T around $T = 0.333\,067$. The simulations use the worm Monte Carlo algorithm described in Sec. III A 2. The finite-size scaling for the finite-temperature phase transition of 3D Villain model is performed by fitting the Monte Carlo data of wrapping probabilities R_x, R_a, and R_2 to (24), of scaled SF stiffness ρ_sL to (28), and of susceptibilitylike quantity T_w to (32). These fits are carried out with the least squares method. For a preferred fit, one expects that χ^2 per degree of freedom (DF) χ^2/DF is $O(1)$. Moreover, for a precaution against systematic errors brought about by the exclusion of high-order correction terms, we prefer the fits

TABLE VII. Fits of T_w to (33) at the estimated critical temperature $T_c = 0.333\,0670\,39$ of the 3D Villain model. The correction exponent $\omega_2 = 1.77$ is adopted. Some of the fits are performed with fixed $\mathcal{Q}_0 = 1.355\,75$ which is determined from Table IV.

$L_{\min}$	χ^2/DF	η	$\mathcal{Q}_0$	b_1	ω_1	b_2
20	13.3/11	0.038 59(16)	1.356(1)	−0.288(7)	0.789	–
24	13.3/10	0.038 59(19)	1.356(1)	−0.289(9)	0.789	–
32	13.2/9	0.038 55(23)	1.356(2)	−0.29(1)	0.789	–
48	11.6/7	0.038 60(31)	1.356(3)	−0.29(2)	0.789	–
12	17.7/12	0.038 45(23)	1.355(2)	−0.27(2)	0.789	−0.23(9)
16	16.8/11	0.038 29(28)	1.354(2)	−0.26(2)	0.789	−0.4(2)
20	13.3/10	0.038 65(34)	1.357(3)	−0.29(3)	0.789	0.1(3)
24	13.2/9	0.038 68(40)	1.357(3)	−0.30(4)	0.789	0.1(4)
20	14.5/11	0.038 53(4)	1.355 75	−0.29(2)	0.791(20)	–
24	14.5/10	0.038 53(5)	1.355 75	−0.29(2)	0.790(27)	–
32	14.3/9	0.038 51(7)	1.355 75	−0.27(3)	0.776(39)	–
48	12.8/7	0.038 52(9)	1.355 75	−0.27(7)	0.776(69)	–
12	18.8/12	0.038 51(7)	1.355 75	−0.25(4)	0.760(46)	−0.3(2)
16	17.0/11	0.038 45(9)	1.355 75	−0.19(5)	0.694(68)	−0.7(3)
20	14.5/10	0.038 53(9)	1.355 75	−0.3(1)	0.790(94)	0.0(6)
24	14.5/9	0.038 53(11)	1.355 75	−0.3(1)	0.79(12)	0.0(9)

with a stability against varying the cutoff size $L_{\min}$, which denotes the smallest lattice of which the data are included in.

We quote the leading correction exponent $\omega_1 = 0.789(11)$ predicated by a $d = 3$ loop expansion [56] and verified by a finite-size scaling of Monte Carlo data [11] that produced $\omega = 0.785(20)$. We shall perform a test for this correction exponent in below. As for the subleading correction term, we adopt the correction exponent $\omega_2 = 1.77$ [56]. We observe that the incorporating of correction terms stabilizes fits. In Table III, we list the details of the fits for dimensionless quantities R_x, R_a, R_2, and $\rho_s L$. The fitting results for T_w are given by Table IV. It is found that the amplitudes of leading correction (namely, $|b_1|$) for these quantities differ from each other. Each of the wrapping probabilities R_x, R_a, and R_2 suffers from minor corrections to scaling, with $|b_1| \lessapprox 0.05$. By contrast, the "conventional" quantity $\rho_s L$ and T_w exhibit more significant corrections with $|b_1| \approx 0.15$ and 0.3, respectively. The distinct amplitudes of finite-size corrections for the quantities can be inferred from Fig. 3.

We should not trust blindly a sole fitting even though χ^2/DF is close to 1 and we do not take any individual fitting result as our final estimate. In fact, we take the medium out of all preferred fitting results of the quantities to estimate T_c. To be conservative, the estimated error bar measures the distance between the final estimate and the farthest bound among those indicated by individual fits. Accordingly, by using the finite-size scaling analyses of the dimensionless quantities and the quantity T_w, respectively, presented in Tables III and IV, we estimate the critical temperature as $T_c = 0.333\,067\,04(7)$. As an illustration, we plot in Fig. 4 the size-dependent behavior of R_x and R_a with correction terms at $T_c = 0.333\,067\,039$ (we take $T_c = 0.333\,067\,04(7)$ and keep one more decimal place) and at its neighborhoods $T = 0.333\,066\,7$ and $0.333\,067\,4$. At T_c, the data becomes asymptotically a constant as $L \to \infty$, whereas it is either upward or downward as T deviates from T_c. These suggest for the present size scale that $T_c = 0.333\,067\,039$ is a reasonable estimate and that $T = 0.333\,0667$ and $0.333\,0674$ deviate from the critical region. The relatively small finite-size corrections of R_x, R_a, and R_2 compared with those of $\rho_s L$ and T_w can be observed in Fig. 5, which demonstrates the corrections to leading scaling for each of the quantities. We determine by Table III (from the estimates of $\mathcal{Q}_0$) the critical wrapping probabilities as $R_x^c = 0.378\,7(2)$, $R_a^c = 0.688\,9(4)$, and $R_2^c = 0.264\,0(3)$, and the critical winding number fluctuations (namely, the critical scaled SF stiffness) as $\rho_s^c L = 0.515\,6(3)$.

2. 3D XY model

By means of the worm algorithm formulated in Sec. III A 1, we simulate the 3D XY model (1) on periodic simple-cubic lattices with linear sizes $L = 8$, 16, 32, 64, 128, 256, 384, and 512 around $T = 2.201\,84$. We aim at

TABLE VIII. Fits of the wrapping probabilities R_x, R_a, R_2 and the scaled SF stiffness $\rho_s L$ to (33) with $y_{\mathcal{Q}} = 0$ at the estimated critical temperature $T_c = 0.333\,067\,039$ of the 3D Villain model. The $\mathcal{Q}_0$'s are fixed at their estimates determined from Table III. The correction exponent $\omega_2 = 1.77$ is adopted.

Qua.	$L_{\min}$	χ^2/DF	$\mathcal{Q}_0$	b_1	ω_1	b_2
R_x	16	4.6/12	0.378 685	−0.034(6)	0.723(40)	−0.10(5)
	20	2.9/11	0.378 685	−0.04(1)	0.769(53)	−0.02(9)
	24	2.9/10	0.378 685	−0.04(2)	0.777(69)	0.0(1)
	32	2.9/9	0.378 685	−0.05(2)	0.78(10)	0.0(3)
R_a	16	4.9/12	0.688 920	−0.025(8)	0.702(71)	0.01(7)
	20	2.2/11	0.688 920	−0.04(2)	0.804(95)	0.2(1)
	24	1.9/10	0.688 920	−0.03(2)	0.76(12)	0.1(2)
	32	1.8/9	0.688 920	−0.04(4)	0.79(18)	0.1(4)
R_2	16	8.6/12	0.264 021	−0.016(4)	0.647(59)	−0.16(4)
	20	8.5/11	0.264 021	−0.015(6)	0.635(77)	−0.18(7)
	24	8.3/10	0.264 021	−0.013(6)	0.603(96)	−0.21(9)
	32	7.8/9	0.264 021	−0.009(6)	0.52(14)	−0.3(2)
$\rho_s L$	16	8.5/12	0.515 565	−0.13(1)	0.767(22)	−0.10(9)
	20	5.3/11	0.515 565	−0.16(2)	0.801(30)	0.1(2)
	24	5.1/10	0.515 565	−0.17(3)	0.812(38)	0.2(3)
	32	4.4/9	0.515 565	−0.21(6)	0.852(59)	0.6(5)

estimating the critical temperature T_c of this paradigmatic model and exploring universal features of critical wrapping probabilities. We fit the quantities R_κ ($\kappa = x, a, 2$) and $\rho_s L$ to their finite-size scaling ansatze (24) and (28), respectively. The fitting results are detailed in Appendix A by which we estimate the critical temperature as $T_c = 2.201\,844\,1(5)$, which is more precise than the best results available in literature, as listed in Table II. The estimate $T_c = 2.201\,844\,1(5)$ is further confirmed by the finite-size scaling analysis with a fixed ν (Appendix A). Figure 6 illustrates the quantities R_x, R_a, $\rho_s L$, and $T_w L^{-2+\eta}$ as a function of T. Shown by Table V, the Villain model and the XY model share universal critical values of wrapping probabilities and of winding number fluctuations.

3. 2D unitary-filling BH model

We extend the applicability of wrapping probability approach to the 2D unitary-filling BH model (8), aiming to precisely locate the U(1) QCP. We simulate the model in canonical ensemble with the worm QMC method within the imaginary-time path-integral representation. The simulations are performed on periodic $L \times L$ lattices with $L = 8$, 16, 32, 48, 64, 80, 96, and 112 for the temperature contour $\beta = 2L$. Particle line wrapping probabilities R_x, R_a, and R_2 together with the SF stiffness ρ_s are sampled. Figure 7 illustrates these quantities around the QCP. Least squares fits are performed for the finite-size scaling analyses described in Sec. III C. It is observed that the sampled wrapping probabilities R_x, R_a, and R_2 all exhibit slight finite-size corrections with the amplitudes of leading correction $|b_1| \lessapprox 0.04$. By contrast, the scaled SF stiffness $\rho_s L$ demonstrates more significant corrections with the amplitude $|b_1| \approx 0.2$. The observation of small corrections for the wrapping probabilities is reminiscent of that for the aforementioned 3D classical models. The fitting results are summarized in Appendix B by which we estimate the critical hopping amplitude as $(t/U)_c = 0.059\,729\,1(8)$.

B. Determining critical exponents ν and η

Estimating critical exponents by performing fits at the precise critical temperature T_c takes the advantage of reducing a fitting parameter. We perform extensive simulations with a number of lattice sizes ($L = 12$, 16, 20, 24, 32, 40, 48, 64, 80, 96, 128, 160, 192, 256, 384, and 512) right at the high-precision critical temperature $T_c = 0.333\,067\,039$ of the 3D Villain model. For a quantity $\mathcal{Q}$ ($\mathcal{Q} = G_{R_xE}$, G_{R_aE}, G_{R_2E}, G_{ρ_sE}, T_w), the scaling ansatz reduces to

$$\mathcal{Q} = L^{y_\mathcal{Q}}\left(\mathcal{Q}_0 + \sum_m b_m L^{-\omega_m}\right), \tag{33}$$

with $y_\mathcal{Q} = 1/\nu$ for G_{R_xE}, G_{R_aE} and G_{R_2E}, $y_\mathcal{Q} = -1 + 1/\nu$ for G_{ρ_sE}, and $y_\mathcal{Q} = 2 - \eta$ for T_w.

TABLE IX. Fits of the wrapping probabilities R_x, R_a, R_2 to (24) and the scaled SF stiffness $\rho_s L$ to (28) for the 3D XY model. The correction exponents $\omega_1 = 0.789$ and $\omega_2 = 1.77$ are adopted.

Qua.	$L_{\min}$	χ^2/DF	T_c	$1/\nu$	$\mathcal{Q}_0$	a_1	b_1	b_2
R_x	16	28.4/31	2.201 844 12(13)	1.58(7)	0.378 70(5)	0.06(2)	−0.030 7(7)	–
	32	26.8/26	2.201 844 12(15)	1.59(8)	0.378 69(8)	0.06(2)	−0.031(2)	–
	64	25.3/21	2.201 844 05(19)	1.57(8)	0.378 8(1)	0.06(2)	−0.033(4)	–
	128	16.9/15	2.201 844 00(33)	1.60(9)	0.378 8(4)	0.05(2)	−0.04(2)	–
	8	30.1/35	2.201 844 01(14)	1.59(8)	0.378 80(7)	0.05(2)	−0.034(1)	0.041(9)
	16	28.4/30	2.201 844 11(17)	1.58(8)	0.378 7(1)	0.06(2)	−0.031(3)	0.00(4)
	32	26.3/25	2.201 844 01(23)	1.58(8)	0.378 8(2)	0.06(2)	−0.037(9)	0.1(2)
R_a	16	31.8/31	2.201 844 47(13)	1.59(8)	0.688 61(8)	0.07(3)	−0.015(1)	–
	32	26.8/26	2.201 844 32(15)	1.62(8)	0.688 8(1)	0.06(3)	−0.019(2)	–
	64	24.4/21	2.201 844 16(20)	1.61(8)	0.689 0(2)	0.07(3)	−0.027(6)	–
	128	17.2/15	2.201 844 15(34)	1.63(9)	0.689 0(5)	0.06(3)	−0.03(2)	–
	8	31.8/35	2.201 844 07(14)	1.62(8)	0.689 1(1)	0.06(3)	−0.033(2)	0.21(1)
	16	27.1/30	2.201 844 23(17)	1.61(8)	0.688 9(2)	0.06(3)	−0.026(5)	0.12(6)
	32	25.1/25	2.201 844 09(24)	1.61(8)	0.689 2(3)	0.07(3)	−0.04(1)	0.4(3)
R_2	16	38.6/31	2.201 844 05(17)	1.62(10)	0.264 09(6)	0.04(2)	−0.023 7(7)	–
	32	30.0/26	2.201 844 25(20)	1.60(10)	0.263 97(8)	0.04(2)	−0.021(2)	–
	64	24.4/21	2.201 843 98(27)	1.57(10)	0.264 2(1)	0.05(3)	−0.027(4)	–
	128	16.0/15	2.201 844 27(45)	1.63(11)	0.263 9(4)	0.04(2)	−0.01(2)	–
	8	40.8/35	2.201 844 08(18)	1.61(10)	0.264 07(7)	0.04(2)	−0.023(1)	−0.002(9)
	16	35.9/30	2.201 844 29(22)	1.60(10)	0.263 9(1)	0.04(2)	−0.018(3)	−0.06(4)
	32	27.8/25	2.201 843 89(32)	1.59(10)	0.264 3(2)	0.04(2)	−0.04(1)	0.3(2)
$\rho_s L$	16	32.9/31	2.201 844 19(14)	1.58(8)	0.515 6(1)	0.11(5)	−0.098(1)	–
	32	26.7/26	2.201 844 13(16)	1.59(8)	0.515 7(2)	0.10(4)	−0.100(3)	–
	64	23.9/21	2.201 843 92(22)	1.59(8)	0.516 0(3)	0.10(5)	−0.112(8)	–
	128	15.9/15	2.201 844 15(35)	1.68(10)	0.515 5(7)	0.06(3)	−0.09(3)	–
	8	33.4/35	2.201 843 98(15)	1.59(8)	0.515 9(1)	0.10(5)	−0.109(3)	0.14(2)
	16	31.8/30	2.201 844 07(18)	1.59(8)	0.515 8(2)	0.10(5)	−0.104(7)	0.08(8)
	32	24.7/25	2.201 843 84(26)	1.58(8)	0.516 2(4)	0.10(5)	−0.13(2)	0.5(4)

We estimate the critical exponent ν from the derivatives of wrapping probabilities $G_{R_\kappa E}$ ($\kappa = x, a, 2$) and the derivative of SF stiffness $G_{\rho_s E}$ by fitting them to (33). The details of the least squares fits are given in Table VI. We find that the amplitudes of leading corrections for $G_{R_x E}$, $G_{R_a E}$, and $G_{R_2 E}$ are typically smaller than that for $G_{\rho_s E}$, even though leading corrections are clearly there for $G_{R_a E}$ and $G_{R_2 E}$. Moreover, it is hard to detect a finite amplitude of leading correction for $G_{R_x E}$, which should be very small if nonzero. This is a useful feature for locating ν as the leading correction term can be precluded out for the less uncertainties of fitting parameters. By fitting $G_{R_x E}$ to (33) without correction term, we determine $\nu = 0.671\,83(6)$ for $L_{\min} = 16$, $\nu = 0.671\,80(8)$ for $L_{\min} = 20$, $\nu = 0.671\,87(9)$ for $L_{\min} = 24$, $\nu = 0.671\,89(11)$ for $L_{\min} = 32$, $\nu = 0.671\,75(14)$ for $L_{\min} = 40$, and $\nu = 0.671\,84(15)$ for $L_{\min} = 48$, with $\chi^2/\mathrm{DF} \approx 1$ for all of these fits. Note that the fitting is already stable as $L_{\min} \gtrapprox 16$. On this basis, we estimate, more or less conservatively, that $\nu = 0.671\,83(18)$. As an illustrative test of our estimate of ν, we plot in Fig. 8(a) the scaled quantity $G_{R_x E} L^{-1/\nu}$ (without correction term) at T_c with $\nu = 0.671\,83$ and find that $G_{R_x E} L^{-1/\nu}$ converges fast. By contrast, the experimental estimate $\nu = 0.670\,9$ [18] is ruled out. Hence, our estimate of ν is further evidenced. For $G_{R_a E}$, $G_{R_2 E}$, and $G_{\rho_s E}$, correction terms are needed to achieve a stable fitting, bringing about more uncertainties for fitting parameters.

In order to estimate η, we fit the finite-size T_w data to (33) with $y_{\mathcal{Q}} = 2 - \eta$. Obvious corrections to scaling are present in the finite-size scaling. We explore the situations with different combinations of correction terms and the situations with $\mathcal{Q}_0$ being fixed or unfixed. By comparing all the fitting results listed in Table VII, our final estimate is $\eta = 0.038\,53(48)$. The scaled quantity $T_w L^{-2+\eta}$ with a leading correction term is shown in Fig. 8(b) for $\eta = 0.038\,53$.

On the basis of the fits for T_w (Table VII), the leading correction exponent is estimated as $\omega_1 = 0.77(13)$, which is consistent with the literature results $\omega_1 = 0.789(11)$ [56] and $\omega_1 = 0.785(20)$ [11]. Besides, we estimate the leading correction exponent ω_1 from the finite-size scaling of quantities R_x, R_a, R_2, and $\rho_s L$, according to (33), with $y_{\mathcal{Q}} = 0$. As shown by Table VIII, we obtain $\omega_1 \approx 0.7$ which agrees with the estimate $\omega_1 = 0.77(13)$ from analyzing T_w.

V. SUMMARY

In this work we utilize the geometric wrapping probability to exploit the quantitative aspects of the U(1) criticality in three dimensions in the contexts of the finite-

TABLE X. Fits of the wrapping probabilities R_x, R_a, R_2 to (24) and the scaled SF stiffness $\rho_s L$ to (28) for the 3D XY model. The critical exponent ν is fixed at our final estimate 0.671 83 for a consistent check of the fits with unfixed ν (Table IX). The correction exponents $\omega_1 = 0.789$ and $\omega_2 = 1.77$ are adopted.

Qua.	$L_{\min}$	χ^2/DF	T_c	$1/\nu$	$\mathcal{Q}_0$	a_1	b_1	b_2
R_x	16	30.0/32	2.201 844 13(13)	1/0.67183	0.378 68(5)	0.095(4)	−0.0305(7)	–
	32	28.5/27	2.201 844 15(16)	1/0.67183	0.378 66(8)	0.095(4)	−0.030(2)	–
	64	26.6/22	2.201 844 05(21)	1/0.67183	0.378 7(1)	0.095(4)	−0.033(4)	–
	128	18.6/16	2.201 843 92(38)	1/0.67183	0.378 9(4)	0.094(4)	−0.04(2)	–
	8	31.8/36	2.201 844 02(15)	1/0.67183	0.378 77(7)	0.094(4)	−0.034(1)	0.040(9)
	16	30.0/31	2.201 844 14(18)	1/0.67183	0.378 7(1)	0.095(4)	−0.030(3)	0.00(4)
	32	27.9/26	2.201 844 00(25)	1/0.67183	0.378 8(2)	0.094(4)	−0.04(1)	0.1(2)
R_a	16	33.6/32	2.201 844 52(14)	1/0.67183	0.688 57(8)	0.132(5)	−0.015(1)	–
	32	29.4/27	2.201 844 37(17)	1/0.67183	0.688 7(1)	0.131(5)	−0.019(2)	–
	64	26.6/22	2.201 844 17(22)	1/0.67183	0.689 0(2)	0.130(6)	−0.027(6)	–
	128	19.5/16	2.201 844 07(40)	1/0.67183	0.689 1(6)	0.130(6)	−0.03(2)	–
	8	34.5/36	2.201 844 08(16)	1/0.67183	0.689 1(1)	0.129(5)	−0.032(2)	0.21(1)
	16	29.6/31	2.201 844 27(19)	1/0.67183	0.688 9(2)	0.130(5)	−0.025(5)	0.11(6)
	32	27.4/26	2.201 844 08(27)	1/0.67183	0.689 2(3)	0.130(6)	−0.04(1)	0.4(3)
R_2	16	40.3/32	2.201 844 05(18)	1/0.67183	0.264 07(6)	0.076(4)	−0.0235(7)	–
	32	31.3/27	2.201 844 29(21)	1/0.67183	0.263 94(8)	0.077(4)	−0.020(2)	–
	64	25.2/22	2.201 843 99(29)	1/0.67183	0.264 2(2)	0.076(4)	−0.027(5)	–
	128	17.5/16	2.201 844 23(53)	1/0.67183	0.263 9(4)	0.076(4)	−0.02(2)	–
	8	42.5/36	2.201 844 10(20)	1/0.67183	0.264 05(7)	0.076(4)	−0.023(1)	−0.003(9)
	16	37.2/31	2.201 844 35(24)	1/0.67183	0.263 9(1)	0.077(4)	−0.017(3)	−0.07(4)
	32	28.9/26	2.201 843 87(35)	1/0.67183	0.264 3(2)	0.076(4)	−0.04(1)	0.3(2)
$\rho_s L$	16	34.2/32	2.201 844 20(14)	1/0.67183	0.515 5(1)	0.178(7)	−0.097(1)	–
	32	28.4/27	2.201 844 14(17)	1/0.67183	0.515 6(2)	0.177(7)	−0.099(3)	–
	64	25.3/22	2.201 843 89(24)	1/0.67183	0.516 0(3)	0.175(7)	−0.112(9)	–
	128	19.9/16	2.201 843 96(43)	1/0.67183	0.515 9(8)	0.174(8)	−0.10(3)	–
	8	34.9/36	2.201 843 97(16)	1/0.67183	0.515 9(1)	0.176(7)	−0.109(3)	0.13(2)
	16	33.3/31	2.201 844 07(20)	1/0.67183	0.515 7(2)	0.177(7)	−0.103(7)	0.07(8)
	32	26.0/26	2.201 843 79(29)	1/0.67183	0.516 3(5)	0.175(7)	−0.13(2)	0.6(4)

temperature transitions in Villain and XY models and the quantum phase transition in the BH model. For both the classical and quantum models, we observe that certain wrapping probability-related quantities exhibit weak corrections in the finite-size scaling. The critical temperatures of the 3D XY and Villain models are estimated as $T_c = 2.201\,844\,1(5)$ and $0.333\,067\,04(7)$, respectively. The QCP of the 2D unitary-filling BH model is estimated as $(t/U)_c = 0.059\,729\,1(8)$. As demonstrated by Table II, our locations of critical points for the 3D XY, 3D Villain, and 2D unitary-filling BH models significantly improve over the best literature results. For the 3D classical models, the universal critical wrapping probabilities are determined as $R_x^c = 0.378\,7(2)$, $R_a^c = 0.688\,9(4)$, and $R_2^c = 0.264\,0(3)$, which have not yet been reported. The critical winding number fluctuation is estimated as $\rho_s^c L = 0.515\,6(3)$, which agrees well with $\rho_s^c L = 0.516\,0(6)$ reported in Ref. [12] and has a better precision. Moreover, we find that the derivative of a wrapping probability with respect to T, namely G_{R_xE}, suffers from negligible corrections. Making use of this feature, we determine the correlation length critical exponent as $\nu = 0.671\,83(18)$, which is comparable with the most precise results available in literature (Table I). In addition, we estimate the critical exponent η as $\eta = 0.038\,53(48)$, which is close to the recent conformal bootstrap result $\eta = 0.038\,52(64)$ [17]. To sum up, this work is a reference for applying wrapping probability-related quantities to determine the quantitative aspects of critical behaviors and provides several benchmarks for the 3D U(1) criticality.

ACKNOWLEDGMENTS

This work was supported by the National Natural Science Foundation of China under Grant No. 11774002 (W.X., Y.S., and J.P.L.) and the National Science Fund for Distinguished Young Scholars under Grant No. 11625522 (Y.D.).

APPENDIX A: FINITE-SIZE SCALING FOR THE THERMODYNAMIC PHASE TRANSITION OF THE 3D XY MODEL

The finite-size scaling of the dimensionless quantities R_x, R_a, R_2, and $\rho_s L$ for the 3D XY model are detailed in Table IX. For each quantity, the least squares fit with a leading correction term is performed. In some cases, a subleading correction term is further included. The leading correction amplitudes are found to be $|b_1| \approx 0.03$, 0.03, and 0.02 for wrapping probabilities R_x, R_a, and R_2, respectively. For $\rho_s L$, we observe more significant corrections with the amplitude $|b_1| \approx 0.1$. By comparing the fitting results of the dimensionless quantities, our final estimate of critical temperature is $T_c = 2.201\,844\,1(5)$.

In Table X, we present the fitting results of the dimensionless quantities with ν being fixed at our final estimate $\nu = 0.671\,83$. These fits produce an estimate of T_c as $2.201\,844\,1(6)$, which is consistent with $T_c = 2.201\,844\,1(5)$ obtained by the fits without a prior knowledge of ν (Table IX).

TABLE XI. Fits of the wrapping probabilities R_x, R_a, R_2 to (24) and the scaled SF stiffness $\rho_s L$ to (28) for the 2D unitary-filling BH model. The correction exponents $\omega_1 = 0.789$ and $\omega_2 = 1.77$ are adopted.

Qua.	$L_{\min}$	χ^2/DF	$(t/U)_c$	$1/\nu$	$\mathcal{Q}_0$	a_1	b_1	b_2
	48	31.0/28	0.059 728 85(22)	1.39(13)	0.205 0(2)	−3(2)	–	–
	64	25.9/20	0.059 729 00(26)	1.39(16)	0.205 2(3)	−3(2)	–	–
R_x	16	34.2/43	0.059 729 08(18)	1.464(44)	0.206 0(2)	−2.0(4)	−0.020(2)	–
	32	32.1/35	0.059 729 33(35)	1.452(87)	0.206 5(7)	−2.1(8)	−0.028(9)	–
	8	37.4/50	0.059 729 21(21)	1.467(38)	0.206 3(3)	−2.0(3)	−0.027(4)	0.06(2)
	16	33.5/42	0.059 729 40(43)	1.465(44)	0.207(1)	−2.0(4)	−0.04(2)	0.2(2)
	48	24.5/28	0.059 729 01(23)	1.41(13)	0.336 1(3)	−4(2)	–	–
	64	20.3/20	0.059 729 14(27)	1.40(16)	0.336 3(4)	−4(3)	–	–
R_a	16	31.0/43	0.059 728 98(17)	1.467(41)	0.336 6(3)	−3.0(5)	−0.016(3)	–
	32	27.1/35	0.059 729 40(34)	1.453(79)	0.338(1)	−3(1)	−0.03(1)	–
	8	32.4/50	0.059 729 23(20)	1.471(37)	0.337 6(5)	−2.9(4)	−0.037(6)	0.18(3)
	16	29.0/42	0.059 729 50(41)	1.470(41)	0.339(2)	−2.9(5)	−0.06(3)	0.4(3)
	48	32.3/28	0.059 728 25(35)	1.22(20)	0.073 9(2)	−3(2)	–	–
	64	23.9/20	0.059 728 64(41)	1.31(25)	0.074 1(2)	−2(2)	–	–
R_2	16	36.2/43	0.059 729 28(27)	1.459(77)	0.075 3(2)	−1.0(3)	−0.023(2)	–
	32	34.1/35	0.059 729 03(54)	1.45(13)	0.075 0(5)	−1.1(6)	−0.020(7)	–
	8	41.4/50	0.059 729 04(32)	1.466(55)	0.074 9(3)	−1.0(2)	−0.017(3)	−0.06(1)
	16	35.9/42	0.059 728 99(66)	1.463(77)	0.074 9(8)	−1.0(3)	−0.02(2)	−0.07(15)
	48	34.3/28	0.059 728 88(28)	1.24(15)	0.981(1)	−27(17)	–	–
	64	28.4/20	0.059 729 08(35)	1.19(18)	0.982(2)	−34(27)	–	–
$\rho_s L$	16	44.8/43	0.059 729 12(19)	1.477(50)	0.989(1)	−10(2)	−0.18(1)	–
	32	41.1/35	0.059 729 60(39)	1.429(86)	0.994(4)	−12(4)	−0.25(5)	–
	8	48.3/50	0.059 729 30(23)	1.488(40)	0.992(2)	−9(2)	−0.24(2)	0.5(1)
	16	43.0/42	0.059 729 65(45)	1.480(50)	0.996(6)	−10(2)	−0.3(1)	1(1)

TABLE XII. Fits of the wrapping probabilities R_x, R_a, R_2 to (24) and the scaled SF stiffness $\rho_s L$ to (28) for the 2D unitary-filling BH model. The critical exponent ν is fixed at our final estimate 0.671 83 for a consistent check of the fits with unfixed ν (Table XI). The correction exponents $\omega_1 = 0.789$ and $\omega_2 = 1.77$ are adopted.

Qua.	$L_{\min}$	χ^2/DF	$(t/U)_c$	$1/\nu$	$\mathcal{Q}_0$	a_1	b_1	b_2
	48	31.6/29	0.059 728 78(18)	1/0.67183	0.205 0(2)	−1.80(4)	–	–
	64	26.2/21	0.059 728 94(22)	1/0.67183	0.205 1(2)	−1.80(4)	–	–
R_x	16	34.5/44	0.059 729 05(17)	1/0.67183	0.205 9(2)	−1.80(3)	−0.020(2)	–
	32	32.2/36	0.059 729 29(32)	1/0.67183	0.206 4(6)	−1.80(4)	−0.027(9)	–
	8	37.7/51	0.059 729 18(20)	1/0.67183	0.206 3(3)	−1.81(3)	−0.027(4)	0.06(2)
	16	33.8/43	0.059 729 37(41)	1/0.67183	0.207(1)	−1.80(3)	−0.04(2)	0.2(2)
	48	24.9/29	0.059 728 94(18)	1/0.67183	0.336 0(3)	−2.71(6)	–	–
	64	20.6/21	0.059 729 07(22)	1/0.67183	0.336 2(3)	−2.70(6)	–	–
R_a	16	31.3/44	0.059 728 95(16)	1/0.67183	0.336 5(3)	−2.72(5)	−0.016(3)	–
	32	27.3/36	0.059 729 35(32)	1/0.67183	0.337 8(9)	−2.71(6)	−0.03(1)	–
	8	32.6/51	0.059 729 21(19)	1/0.67183	0.337 6(5)	−2.72(5)	−0.036(6)	0.18(3)
	16	29.2/43	0.059 729 48(40)	1/0.67183	0.339(2)	−2.71(5)	−0.06(3)	0.4(3)
	48	34.1/29	0.059 728 19(28)	1/0.67183	0.073 9(1)	−0.90(3)	–	–
	64	24.4/21	0.059 728 57(34)	1/0.67183	0.074 1(2)	−0.89(3)	–	–
R_2	16	36.3/44	0.059 729 26(26)	1/0.67183	0.075 3(2)	−0.90(3)	−0.023(1)	–
	32	34.2/36	0.059 728 99(50)	1/0.67183	0.075 0(5)	−0.89(3)	−0.019(7)	–
	8	41.6/51	0.059 729 03(31)	1/0.67183	0.074 9(2)	−0.90(3)	−0.017(3)	−0.06(1)
	16	36.1/43	0.059 728 96(64)	1/0.67183	0.074 8(8)	−0.90(3)	−0.02(2)	−0.1(1)
	48	37.1/29	0.059 728 70(21)	1/0.67183	0.980(1)	−9.4(2)	–	–
	64	31.2/21	0.059 728 86(24)	1/0.67183	0.981(1)	−9.4(2)	–	–
$\rho_s L$	16	44.8/44	0.059 729 10(18)	1/0.67183	0.989(1)	−9.4(2)	−0.18(1)	–
	32	41.6/36	0.059 729 52(35)	1/0.67183	0.993(4)	−9.4(2)	−0.25(5)	–
	8	48.3/51	0.059 729 30(22)	1/0.67183	0.992(2)	−9.4(2)	−0.24(2)	0.5(1)
	16	43.0/43	0.059 729 63(44)	1/0.67183	0.996(6)	−9.4(2)	−0.3(1)	1(1)

APPENDIX B: FINITE-SIZE SCALING FOR THE QUANTUM PHASE TRANSITION OF 2D UNITARY-FILLING BH MODEL

The QCP of the 2D unitary-filling BH model is determined by finite-size scaling analyses of the dimensionless quantities R_x, R_a, R_2, and $\rho_s L$. The details of least squares fits are summarized in Table XI. For each quantity, we perform fits without correction term or with different combinations of leading and subleading correction terms. It is observed that the leading correction amplitudes $|b_1|$ for the wrapping probabilities are $|b_1| \lessapprox 0.04$. For $\rho_s L$, it is found that $|b_1| \approx 0.2$. Note that the leading finite-size corrections of R_x, R_a, and R_2 are considerably smaller than that of $\rho_s L$. By comparing the fitting results in Table XI, we provide the final estimate of QCP as $(t/U)_c = 0.059\,729\,1(8)$.

We also perform fits with fixed critical exponent $\nu = 0.671\,83$. The results are summarized in Table XII, which yields $(t/U)_c = 0.059\,729\,1(7)$, agreeing with the analyses with unfixed ν.

[1] J. M. Kosterlitz and D. J. Thouless, Ordering, metastability and phase transitions in two-dimensional systems, J. Phys. C **6**, 1181 (1973).

[2] B. V. Svistunov, E. S. Babaev, and N. V. Prokof'ev, *Superfluid States of Matter* (CRC Press, Boca Raton, 2015).

[3] M. Hermele, M. P. A. Fisher, and L. Balents, Pyrochlore photons: The $U(1)$ spin liquid in a $S = 1/2$ three-dimensional frustrated magnet, Phys. Rev. B **69**, 064404 (2004).

[4] M. Hermele, T. Senthil, M. P. A. Fisher, P. A. Lee, N. Nagaosa, and X.-G. Wen, Stability of $U(1)$ spin liquids in two dimensions, Phys. Rev. B **70**, 214437 (2004).

[5] T. Senthil, A. Vishwanath, L. Balents, S. Sachdev, and M. P. A. Fisher, Deconfined quantum critical points, Science **303**, 1490 (2004).

[6] T. Senthil, L. Balents, S. Sachdev, A. Vishwanath, and M. P. A. Fisher, Quantum criticality beyond the landau-ginzburg-wilson paradigm, Phys. Rev. B **70**, 144407 (2004).

[7] M. Greiner, O. Mandel, T. Esslinger, T. W. Hänsch, and I. Bloch, Quantum phase transition from a superfluid to a mott insulator in a gas of ultracold atoms, Nature (London) **415**, 39 (2002).

[8] L. D. Faddeev, *Gauge Fields: An Introduction to Quantum Theory* (CRC Press, Boca Raton, 2018).

[9] M. Campostrini, M. Hasenbusch, A. Pelissetto, P. Rossi, and E. Vicari, Critical behavior of the three-dimensional XY universality class, Phys. Rev. B **63**, 214503 (2001).

[10] F. Alet and E. S. Sørensen, Directed geometrical worm algorithm applied to the quantum rotor model, Phys. Rev. E **68**, 026702 (2003).

[11] M. Campostrini, M. Hasenbusch, A. Pelissetto, and E. Vicari, Theoretical estimates of the critical exponents of the superfluid transition in ^{4}He by lattice methods, Phys. Rev. B **74**, 144506 (2006).

[12] E. Burovski, J. Machta, N. Prokof'ev, and B. Svistunov, High-precision measurement of the thermal exponent for the three-dimensional XY universality class, Phys. Rev. B **74**, 132502 (2006).

[13] T.-Y. Lan, Y.-D. Hsieh, and Y.-J. Kao, High-precision monte carlo study of the three-dimensional XY model on gpu, arXiv:1211.0780.

[14] Y. Komura and Y. Okabe, Cuda programs for the gpu computing of the swendsen–wang multi-cluster spin flip algorithm: 2D and 3D ising, potts, and XY models, Comp. Phys. Commun. **185**, 1038 (2014).

[15] A. P. Gottlob, M. Hasenbusch, and S. Meyer, Critical behaviour of the 3D XY-model: A monte carlo study, Nucl. Phys. B **30**, 838 (1993).

[16] M. Campostrini, A. Pelissetto, P. Rossi, and E. Vicari, Determination of the critical exponents for the λ transition of ^{4}He by high-temperature expansion, Phys. Rev. B **61**, 5905 (2000).

[17] F. Kos, D. Poland, D. Simmons-Duffin, and A. Vichi, Precision islands in the ising and $O(N)$ models, J. High Energy Phys. 08 (2016) 036.

[18] J. A. Lipa, J. A. Nissen, D. A. Stricker, D. R. Swanson, and T. C. P. Chui, Specific heat of liquid helium in zero gravity very near the lambda point, Phys. Rev. B **68**, 174518 (2003).

[19] A. Goldman, *Percolation, Localization, and Superconductivity* (Springer Science & Business Media, Berlin, Heidelberg, 2013), Vol. 109.

[20] R. H. Swendsen and J.-S. Wang, Nonuniversal Critical Dynamics in Monte Carlo Simulations, Phys. Rev. Lett. **58**, 86 (1987).

[21] U. Wolff, Collective Monte Carlo Updating for Spin Systems, Phys. Rev. Lett. **62**, 361 (1989).

[22] N. V. Prokof'ev and B. V. Svistunov, Worm Algorithms for Classical Statistical Models, Phys. Rev. Lett. **87**, 160601 (2001).

[23] K. Chen, L. Liu, Y. Deng, L. Pollet, and N. Prokof'ev, Universal Conductivity in a Two-Dimensional Superfluid-to-Insulator Quantum Critical System, Phys. Rev. Lett. **112**, 030402 (2014).

[24] W. Witczak-Krempa, E. S. Sørensen, and S. Sachdev, The dynamics of quantum criticality revealed by quantum monte carlo and holography, Nat. Phys. **10**, 361 (2014).

[25] O. Dutta, M. Gajda, P. Hauke, M. Lewenstein, D. Lühmann, B. A. Malomed, T. Sowiński, and J. Zakrzewski, Non-standard hubbard models in optical lattices: A review, Rep. Prog. Phys. **78**, 066001 (2015).

[26] S. Trotzky, L. Pollet, F. Gerbier, U. Schnorrberger, I. Bloch, N. V. Prokof'ev, B. Svistunov, and M. Troyer, Suppression of the critical temperature for superfluidity near the mott transition, Nat. Phys. **6**, 998 (2010).

[27] M. Endres, M. Cheneau, T. Fukuhara, C. Weitenberg, P. Schauß, C. Gross, L. Mazza, M. C. Banuls, L. Pollet, I. Bloch *et al.*, Observation of correlated particle-hole pairs and string order in low-dimensional mott insulators, Science **334**, 200 (2011).

[28] N. Elstner and H. Monien, Dynamics and thermodynamics of the bose-hubbard model, Phys. Rev. B **59**, 12184 (1999).

[29] B. Capogrosso-Sansone, Ş. Söyler, N. V. Prokof'ev, and B. V. Svistunov, Monte carlo study of the two-dimensional bose-hubbard model, Phys. Rev. A **77**, 015602 (2008).

[30] J. A. Lipa, D. R. Swanson, J. A. Nissen, T. C. P. Chui, and U. E. Israelsson, Heat Capacity and Thermal Relaxation of Bulk Helium very Near the Lambda Point, Phys. Rev. Lett. **76**, 944 (1996).

[31] Y. Deng, H. W. J. Blöte, and M. P. Nightingale, Surface and bulk transitions in three-dimensional $O(N)$ models, Phys. Rev. E **72**, 016128 (2005).

[32] H. G. Ballesteros, L. A. Fernandez, V. Martin-Mayor, and A. M. Sudupe, Finite size effects on measures of critical exponents in $d = 3$ $O(N)$ models, Phys. Lett. B **387**, 125 (1996).

[33] A. Cucchieri, J. Engels, S. Holtmann, T. Mendes, and T. Schulze, Universal amplitude ratios from numerical studies of the three-dimensional $O(2)$ model, J. Phys. A: Math. Gen. **35**, 6517 (2002).

[34] F. Alet and E. S. Sørensen, Cluster monte carlo algorithm for the quantum rotor model, Phys. Rev. E **67**, 015701(R) (2003).

[35] M. C. Cha, M. P. A. Fisher, S. M. Girvin, M. Wallin, and A. P. Young, Universal conductivity of two-dimensional films at the superconductor-insulator transition, Phys. Rev. B **44**, 6883 (1991).

[36] J. Šmakov and E. Sørensen, Universal Scaling of the Conductivity at the Superfluid-Insulator Phase Transition, Phys. Rev. Lett. **95**, 180603 (2005).

[37] H. Nishimori and G. Ortiz, *Elements of Phase Transitions and Critical Phenomena* (OUP Oxford, Oxford, 2010).

[38] Y. Deng, T. M. Garoni, and A. D. Sokal, Dynamic Critical Behavior of the Worm Algorithm for the Ising Model, Phys. Rev. Lett. **99**, 110601 (2007).

[39] N. V. Prokof'ev, B. V. Svistunov, and I. S. Tupitsyn, Exact, complete, and universal continuous-time worldline monte carlo approach to the statistics of discrete quantum systems, J. Exp. Theor. Phys. **87**, 310 (1998).

[40] N. V. Prokof'ev, B. V. Svistunov, and I. S. Tupitsyn, "worm" algorithm in quantum monte carlo simulations, Phys. Lett. A **238**, 253 (1998).

[41] N. V. Prokof'ev and B. V. Svistunov, Worm algorithm for problems of quantum and classical statistics, arXiv:0910.1393.

[42] L. Pollet, Recent developments in quantum monte carlo simulations with applications for cold gases, Rep. Prog. Phys. **75**, 094501 (2012).

[43] J.-P. Lv, Y. Deng, and Q.-H. Chen, Worm-type monte carlo simulation of the ashkin-teller model on the triangular lattice, Phys. Rev. E **84**, 021125 (2011).

[44] R. P. Langlands, C. Pichet, P. Pouliot, and Y. Saint-Aubin, On the universality of crossing probabilities in two-dimensional percolation, J. Stat. Phys. **67**, 553 (1992).

[45] H. T. Pinson, Critical percolation on the torus, J. Stat. Phys. **75**, 1167 (1994).

[46] R. M. Ziff, C. D. Lorenz, and P. Kleban, Shape-dependent universality in percolation, Physica A **266**, 17 (1999).

[47] M. E. J. Newman and R. M. Ziff, Fast monte carlo algorithm for site or bond percolation, Phys. Rev. E **64**, 016706 (2001).

[48] L. P. Arguin, Homology of fortuin–kasteleyn clusters of potts models on the torus, J. Stat. Phys. **109**, 301 (2002).

[49] P. H. L. Martins and J. A. Plascak, Percolation on two- and three-dimensional lattices, Phys. Rev. E **67**, 046119 (2003).

[50] J. Wang, Z. Zhou, W. Zhang, T. M. Garoni, and Y. Deng, Bond and site percolation in three dimensions, Phys. Rev. E **87**, 052107 (2013).

[51] X. Xu, J. Wang, J.-P. Lv, and Y. Deng, Simultaneous analysis of three-dimensional percolation models, Front. Phys. **9**, 113 (2014).

[52] P. Hou, S. Fang, J. Wang, H. Hu, and Y. Deng, Geometric properties of the fortuin-kasteleyn representation of the ising model, Phys. Rev. E **99**, 042150 (2019).

[53] E. L. Pollock and D. M. Ceperley, Path-integral computation of superfluid densities, Phys. Rev. B **36**, 8343 (1987).

[54] M. P. A. Fisher, P. B. Weichman, G. Grinstein, and D. S. Fisher, Boson localization and the superfluid-insulator transition, Phys. Rev. B **40**, 546 (1989).

[55] M. Ma, B. I. Halperin, and P. A. Lee, Strongly disordered superfluids: Quantum fluctuations and critical behavior, Phys. Rev. B **34**, 3136 (1986).

[56] R. Guida and J. Zinn-Justin, Critical exponents of the *N*-vector model, J. Phys. A: Math. Gen. **31**, 8103 (1998).